iScience

CellPress
OPEN ACCESS

Article

Ultra-sensitive terahertz metamaterials biosensor based on luxuriant gaps structure

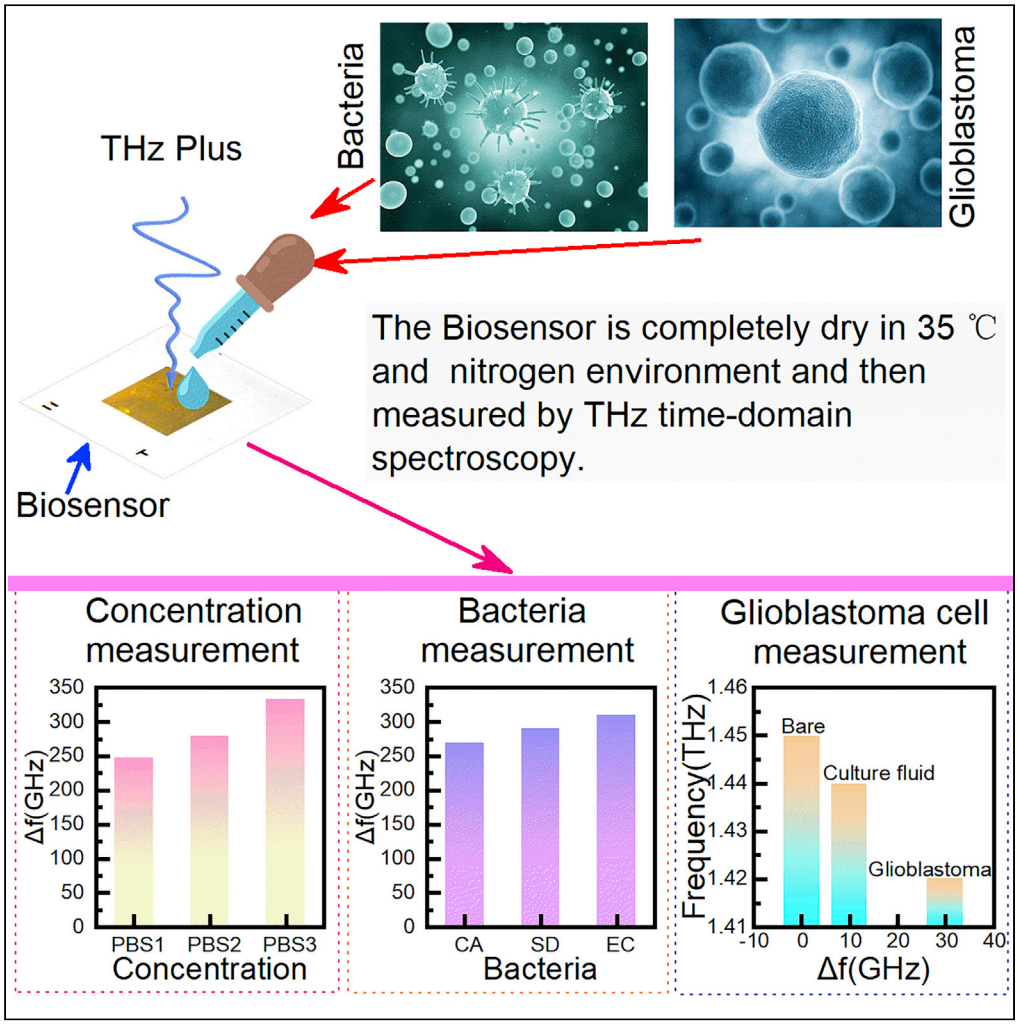

KangLong Chen, Cunjun Ruan, Fangyuan Zhan, Xiaoyu Song, Ayesha Kosar Fahad, Tianyao Zhang, Wei Shi

ruancunjun@buaa.edu.cn (C.R.)
shiweilab@buaa.edu.cn (W.S.)

Highlights

Biosensor based on luxuriant gaps metamaterial has been proposed

Different concentrations have been successfully detected

Different types of bacteria have been successfully distinguished

This sensor is promising for early diagnosis of glioblastoma

Chen et al., iScience 26, 105781
January 20, 2023
https://doi.org/10.1016/j.isci.2022.105781

iScience

CellPress
OPEN ACCESS

Article

Ultra-sensitive terahertz metamaterials biosensor based on luxuriant gaps structure

KangLong Chen,[1] Cunjun Ruan,[1,2,6,*] Fangyuan Zhan,[3] Xiaoyu Song,[4] Ayesha Kosar Fahad,[1] Tianyao Zhang,[5] and Wei Shi[4,*]

SUMMARY

Fast, simple, and label-free detections and distinctions are desirable in cell biology analysis and diagnosis. Here, a biosensor based on terahertz metamaterial has luxuriant gaps, which can excite dipole resonance is designed. Filling the gaps with various analytes can change the biosensor's capacitance resulting in electromagnetic properties changing. The idea is verified by simulations and experiments. The theoretical sensitivity of the biosensor approaches 290 GHz/RIU, and the experimental concentration sensitivity of the biosensor is $\geq$ 275 kHz mL/cell. Candida Albicans, Escherichia Coli, and Shigella Dysenteriae were selected as analytes, and the measurement frequency shift is 270 GHz, 290 GHz, and 310 GHz, respectively, which indicates that the biosensor can detect and distinguish these bacteria. Successfully detection of low-concentration glioblastoma (200 cells/mL), showing great potential for the early diagnosis of glioblastoma of the biosensor. This biosensor supplies a new horizon for cell detection, which will significantly benefit cell biology investigation.

INTRODUCTION

Detecting and distinguishing cells is the premise of cell biology investigation. Biosensors based on metamaterials (MMs) working in terahertz (THz) meet this growing demand.[1] MMs are artificial electromagnetic materials composed of periodically arranged unit cells, and these unit cells are in subwavelength dimensions.[2,3] The other eight-unit cell is the boundary conditions of the unit cell, which is surrounded by.[4–7] In this case, the electromagnetic (EM) response will be more stable and sensitive to the tiny environmental change, significantly contributing to the biosensor.[8,9] Biological cells put on MMs as analytes can modulate the EM response of MMs mainly by changing the capacitance (C) of MMs; due to C and inductance (L) being the main elements that decide resonance frequency (f), the f follows the equation $f = 1/(2\pi\cdot(LC)^{0.5})$. The unit cell consists of a substrate and metal shape where C is mainly formed by gaps between wires which constitute the shape. Thus, luxuriant gaps can help improve biosensor sensitivity based on MMs. In addition, the electric field is mainly trapped and can be enhanced around the gap, which will further improve the sensitivity.[10,11]

In recent years, many biosensors based on MMs have been reported. A novel biosensor based on electromagnetic-induced transparency-like (EIT-like) MMs has been used to detect oral cancer cells HSC3. Simulation results demonstrate that the maximum theoretical sensitivity can approach 455.71 GHz/RIU. The experiment results show that this biosensor sensitivity approach 900 kHz mL/cell at 7×10^5 cells/mL. Different concentration anti-cancer drug was used to make cancer cells apoptosis, and the extension of drug action time from 24 to 72 h, the Δf changes from 140 to 70 GHz and 140 to 40 GHz. This biosensor supplies a new way to realize fast and low-cost cell detection from a physical perspective.[12] A metamaterial biosensor composed of SRRs and cut wires which can induce an EIT-like resonant peak at 2.24 THz has been proposed. This sensor was employed to classify glioma cells. The theoretical sensitivity of the proposed biosensor can approach 496.01 GHz/RIU. The experimental sensitivity approach is 248.75 kHz mL/cell, enabling sensitive detection of the glioma cells' activity from a physical perspective.[13] EIT-like MMs consisting of a CW and a pair of SRRs have been designed, and the MMs are used as biosensors to detect cancer cell concentration. The theoretical sensitivity of the biosensor based on EIT-like MMs was evaluated up to 248.8 GHz/RIU. In the experiment, A549 cells were selected as the analytes, and the results show that when the cell concentration changes from 0.5×10^5 to 5×10^5 cells/mL, the frequency shift (Δf) increases from 24 to 50 GHz. Any change in cell measurement will result in the lineshape variation in EIT-like MMs.

[1]School of Electronic and Information Engineering, Beihang University, Beijing 100191, China

[2]Beijing Key Laboratory for Microwave Sensing and Security Applications, Beihang University, Beijing 100191, China

[3]Key Laboratory for the Physics and Chemistry of Nano Devices, School of Electronics, Peking University, Beijing 100871, China

[4]School of Engineering Medicine and School of Biological Science and Medical Engineering, Beihang University, Beijing 100191, China

[5]Beijing Engineering Research Center of Industrial Spectrum Imaging, School of Automation and Electrical Engineering, University of Science and Technology Beijing, Beijing 100083, China

[6]Lead contact

*Correspondence: ruancunjun@buaa.edu.cn (C.R.), shiweilab@buaa.edu.cn (W.S.)

https://doi.org/10.1016/j.isci.2022.105781

Such biosensor based on the MMs offers a novel way to obtain fast and low-cost cell detection.[14] These biosensors are all based on EIT-like MMs because the EIT resonance only depends on the non-radiative damping, making the MMs sensitive to the environment.[12] However, some biosensors based on MMs can only excite dipole resonance performing worse than the EIT-like MMs. A biosensor based on antibody-modified THz MMs is proposed to detect the concentration of carcinoembryonic antigen (CEA). The theoretical sensitivity of the MMs is only 76.5 GHz/RIU. When the concentration of Anti-CEA is 20 ng/mL, the resonant frequency shift shows good linearity to the concentration of CEA, and the limit of detection reaches 0.1 ng/mL. This study paves a new way for sensitively detecting cancer biomarkers and immune responses, which is important for early-stage diagnosis of cancers.[15] MMs consist of SRR structures with double splits has been designed for biosensors to detect cancer cells HSC3. The theoretical sensitivity of this biosensor was calculated to 182 GHz/RIU. This biosensor was used to investigate the apoptosis of cancer cells. The results measured by the biological CCK-8 kits method agree with the trend of Δf measured by proposed MMs-based biosensors. This biosensor supplies a picture of cell apoptosis from the physical perspective.[16] The reported biosensors based on EIT-like MMs performed better than dipole model MMs.

In this work, a biosensor based on dipole resonant model THz MMs has been proposed. The MMs is composed of split rings and cross. The optimum thickness of the analyte layer has been numerically calculated, and the results demonstrate that when the thickness is 15 μm, the biosensor can perform best. The theoretical sensitivity of these MMs approached 290 GHz/RIU under the analyte thickness of 15 μm condition. A series of experiments have been carried out to verify this sensor. Firstly, different concentrations of Candida Albicans solution were tested. The concentration varies from 2×10^5 cells/mL, 8×10^5 cells/mL, and 1.2×10^6 cells/mL, the corresponding Δf is 250 GHz, 270 GHz, and 330 GHz, respectively. So, the maximum and minimum experiment sensitivity is 1250 kHz mL/cell, 337.5 kHz mL/cell, and 275 kHz mL/cell, respectively. Secondly, different types of bacteria have been tested. The experiment results demonstrate that with the size of bacteria decreases, the frequency redshifts more, and the Δf of Candida Albicans (CA), Escherichia Coli (EC), and *Shigella dysenteriae* (SD) under 8×10^5 cells/mL concentration conditions is 270 GHz, 290 GHz, and 310 GHz, respectively. This means different types of bacteria can be detected and distinguished. Finally, low-concentration glioblastoma and culture fluid is measured, and each solution can result in at least 10 GHz and 30 GHz frequency shift, respectively. And the frequency shifts between glioblastoma and culture fluid $|\Delta f_g\text{-}\Delta f_c| \geq 20$ GHz means the biosensor can detect and distinguish between glioblastoma and culture fluid. These luxuriate gaps are promising in biological detection.

RESULTS AND DISCUSSION

Design and verification

Split rings and cross combine structures (SRCCS) have been designed, as shown in Figure 1. The cross looks like a coordinate axis, and each split ring lies in each quadrant. In SRCCS, the metal shape is Au with $\sigma = 4.561*10^7$ S/m, and the substrate is quartz (lossy) with $\varepsilon = 3.75$. The parameters are as follows: p = 80 μm, *L1* = 66 μm, *L2* = 24 μm, *D* = 6 μm, *W* = 6 μm, *G* = 5 μm. The thickness of Au is *T* = 0.2 μm, and the substrate is *H* = 1000 μm, respectively. Au is selected as metal shape material due to its good electrical conductivity and stable chemical properties.[17,18]

SRCCS is designed in this shape to increase the capacitance C. We all know that the relationship between resonance frequency *f* between C and inductance L is as follows: $f = 1/(2\pi\times(LC)^{0.5})$. In our structure, there are four split rings. Gaps of split rings will increase the value of C, and gaps between split rings and cross will further result in a C increase. While in this structure, $C=C_{dc} + C_{pc}$, C_{dc} is the distributed capacitance, and C_{pc} is the plate capacitor. And $C_{pc} = \varepsilon_0\varepsilon_r S/d$, here $\varepsilon_0\varepsilon_r$ is the permittivity between the two plates, and S is the area of the plate, d is the distance between the two plates. In our structure, if there is more gap between wires, more analytes can be filled in, which means C can have more dramatic changes. In other words, the structure will be sensitive to the background change. Thus, we design four split rings and make these rings close to the cross to increase C, ensuring this structure is sensitive.

SRCCS has been numerically calculated and measured. Two-side polished, 1 mm thick quartz was used as a substrate for MMs with the help of conventional photolithography, and then 200 nm gold was thermally metalized to form the metallic part of each MMs. The SEM Photograph of MMs' single unit cell is shown in Figure 2A. Using the THz-time domain spectroscopy (TDS), we measured MMs. The simulation and measurement results are shown in Figure 2B.

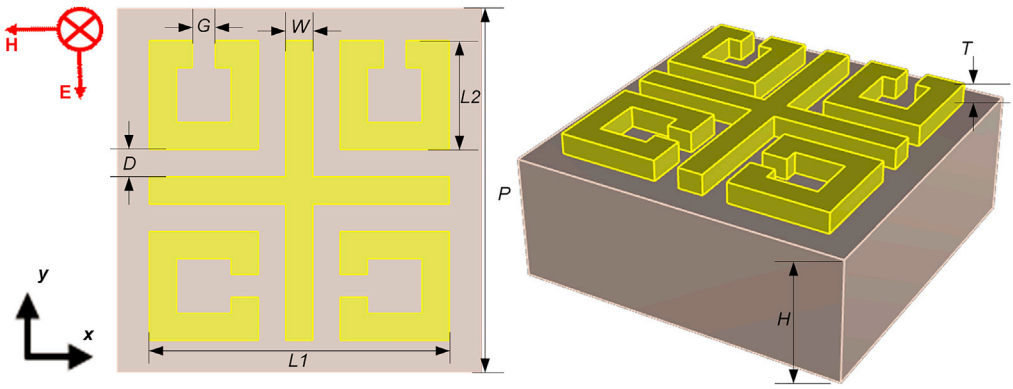

Figure 1. The schematic of the original symmetric SRCCS structure
The top view (left) and side view (right).

The SEM graph shows that fabrication has been perfectly done in close visual agreement with the SEM picture and modeled structure in Figure 1. And the measurement result will confirm it, as shown in Figure 2B. Due to the fabrication technology, there are some errors between fabrication and design, leading to differences between simulation and measurement results. The measurement results indicate that though there is some difference in amplitude in transmission curves, the envelope of measurement results is in close agreement with simulation, except for a resonance peak at around 1.5 THz, which has not been detected due to the high Q-factor of this resonance peak and lack of scanning time.[19] The thickness of the substrate will limit the measurement scanning time. Fortunately, our study does not focus on that resonance peak. Overall, the measurement results are in agreement with the simulation results. In other words, the fabrication conforms to the design.

The electric field and surface current will reveal the physical mechanism of the resonance peak at 1.47 THz. The incident THz wave's electric-field is parallel to the y-direction. We define the cross as a coordinate axis. This structure is symmetric in the y-direction, and the electric-field distributes in the gap, both the tail end of the cross arm in the x-direction and the upper tail end of the cross arm, as shown in Figure 3A. The electric field also distributes symmetrically concerning the y axis. Such electric field will generate dipole resonant mode.[20–24] Meanwhile, the surface current in each split ring will excite magnetic dipoles, as shown in Figure 3B. Coincidentally, the left part split rings, magnetic dipoles' directions opposite the right part. The same condition happens on the cross. So the magnetic dipoles have the same role in producing the resonant mode effect of offsetting each other.[25–28] In a word, unlike the EIT-like resonant excited by quadrupole, such dipole resonant mode is not sensitive and hence maintains its characteristics.

To confirm the sensitivity of these MMs, an analyte layer was put onto the MMs structure and filled in the gap in the metal shape. The theoretically calculated results are shown in Figure 4. The best thickness of the analyte must be confirmed to bring out the best in the use of the MMs' sensitivity. And to ensure thickness is best, we choose as lower refractive index as possible. Thus, the refractive index is fixed at 1.1, and the thickness grows from 1 μm to 18 μm, as shown in Figure 4A. It shows that there is a significant frequency shift (Δf, defined as the absolute value of resonance peak frequency distance between the curve of MMs with analyte layer and bare MMs) under bare and 7 μm, 7 μm-13 μm conditions, the Δf is a remarkable change from 46 GHz to 59 GHz, respectively.

In comparison, Δf grows slowly when thickness increases to 15 μm and 18 μm. The enlarged part in Figure 4A shows that the amplitude increases with analyte layer thickness growing from 13 μm to 18 μm. From Figure 4B, we can find that the absolute value slope factor of the resonance peak frequency line (the pink one) decreases to zero. At the same time, the frequency shift curve (orange one) slope factor also drops to zero. That means when the thickness is 15 μm, the MMs can perform best. Once the optimal thickness is determined, the refractive index of the analyte changes from 1 to 1.6 under the thickness fixed at 15 μm, the simulation results are shown in Figure 4C. The enlarged part in Figure 4C Indicates that the resonance peak frequency redshifts with the refractive index increases and the amplitude lower. Figure 4D shows the linear relationship between resonance peak frequency and Δf, and the corresponding linear fitting curve is given. The two linear fitting curves are almost linear, meaning when the refractive index

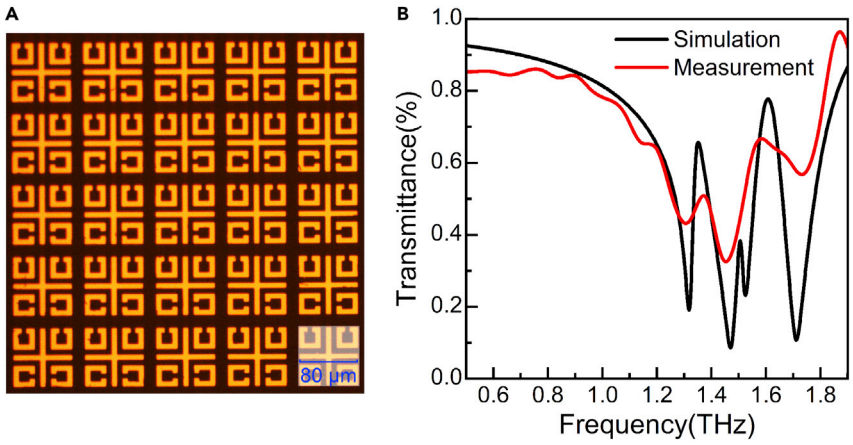

Figure 2. Fabrication, design, and measurement

(A) The SEM photograph of the fabricated MMs.

(B) Simulation and measurement results of terahertz wave electric field in y-direction.

varies per 0.1, the Δf changes about 29 GHz. Namely, the theoretical sensitivity of the refractive index sensor based on our designed MMs approaches 290 GHz/RIU (RIU, Refractive Index Unit).[12–16,29,30] The theoretical sensitivity indicates that the MMs are promising to be used as biosensors.

In our study, we employ the Electric dipole resonance peak as the feature peak to achieve the sensor applications. The sensitivity of the sensor is compared with some reported structures to show the superiority of the design. The comparison results are shown in Table 1.

The comparison results indicate that the proposed structure performance is good as a sensor. The proposed structure sensitivity is better than structures 1, 2, 3, and 5, which can excite dipole resonance. And even superior to some EIT-like resonance and Fano resonance.

Measurement results

Concentration measurement

The bacteria thickness depends on the solution concentration and volume in the experiment. Earlier in the article, 1 mL solution is shifted on the MMs, after that the biosensors will be placed at about 35 °C, and nitrogen environment until these sensors were completely dry, then various thickness analyte sedimentation will form. So that concentration will determine the thickness. Candida Albicans (CA) PBS is chosen as the analyte to carry out the concentration detection experiment. The ability to detect varying concentrations of bacteria is a vital property index of the MMs biosensor. Another property index is that biosensors can detect bacteria in a low concentration. The experiment results are shown in Figure 5.

The transmittance curves in different concentration cases are shown in Figure 5A. These curves are shown in a 3D waterfall plot to make the frequency shift more distinct, the x axis offset is −10, and the y axis offset is −50, so the curve corresponding axis values are incorrect. The exact resonance peak frequency of bare, PBS1 (2×10^5 cells/mL), PBS2 (8×10^5 cells/mL), and PBS3 (1.2×10^6 cells/mL) is 1.45 THz, 1.20 THz, 1.18 THz, and 1.12 THz, respectively, as shown in Figure 5B the pink line. And the Δf of PBS1, PBS2, and PBS3 is 250 GHz, 270 GHz, and 330 GHz, as shown in Figure 5B, the blue line. The measurement results indicate that the resonance peak of MMs is sensitive to the variation of bacteria concentration. It may not be easy to determine the minimum concentration that the MMs biosensor can normally operate. We define the sensitivity of concentration (SoC) = Δf/concentration,[12,13] which means, theoretically, per CA bacteria cell in 1 mL solution can lead the frequency shift. The details are shown in Table 2.

The SoC calculation formula is workable depending on whether the CA cell is evenly distributed in the solution and distributed evenly on the surface of the MMs biosensor. The calculated SoC indicates that each

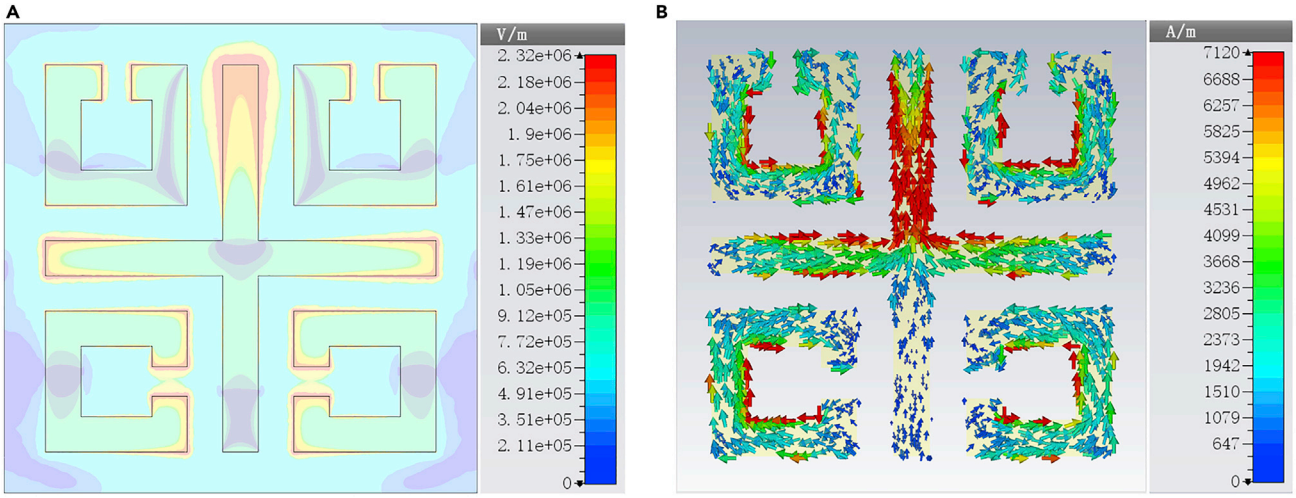

Figure 3. The simulation electromagnetic field of MMS

(A and B) The electric-field (A) and surface current (B) distribution of SRCCS MMs.

CA cell can lead to at least 275 kHz resonance peak frequency shift. This property provides a way to investigate bacteria cells.

Bacteria measurement

Candida Albicans (CA) solution is selected as the analyte to conduct the concentration experiment. The experiment results indicate that the MMs biosensor is sensitive to various concentrations. While under the same concentration condition, the bacteria types may not be the same. So, it is crucial that the MMs biosensor can distinguish different bacteria types.

Candida Albicans (CA), Escherichia Coli (EC), and *S. dysenteriae* (SD) under 8×10^5 cells/mL concentration conditions are selected as analytes. We prepared the MMs biosensor and tested it, and the measurement results are shown in Figure 6. To remove the impacts of amplitude overlap, transmittance curves are demonstrated in amplitude offset, as shown in Figure 6A. There are significant frequency shifts between bare sample and bacteria transmittance curves. The details are shown in Figure 6B. The amplitude follows the theoretically calculated results (as shown in Figure 4C) with the resonance peak frequency redshift, the amplitude is lower, and each resonance peaks are distinguishable. The critical data are extracted and shown in Figure 6C. When CA is shifted on MMs biosensor, the resonance peak frequency dramatically shifts to 1.18 THz, and the Δf is 270 GHz. As to SD, the resonance peak frequency is 1.16 THz, and Δf grows to 290 GHz. The one that the frequency moves the most is EC, Δf can reach about 310 GHz, and the resonance peak frequency lies around 1.14 THz (limited by the resolution of TDS, the maximum resolution is 10 GHz). The critical data implies that the MMs biosensor can detect CA, SD, and EC under the concentration 8×10^5 cells/mL condition. Furthermore, the electromagnetic response difference among CA, SD, and EC are also distinguishable. This means the MMs biosensor can distinguish CA, SD, and EC solutions. The device supplies a non-label and rapid test way to distinguish these bacteria.

The experiment reveals that the bigger the bacteria's size, the smaller the Δf. The reason why Δf and bacteria size move in the opposite direction is because when the solution shifts on MMs biosensor, with the water in the solution going away, the bacteria cells fall into the gaps. In this study, the effect of water has been eliminated. Thus, the smaller the size is, the more cells will fill in these gaps. And the more capacitance C increase, the further the redshift of resonance peaks is. Finally, it results in Δf increase. So, this is the reason why the analyte cell decrease while the Δf increase.

Cancer cell measurement

Gliomas are one of the most deadly brain tumor diseases, and the most common type of glioma is glioblastoma.[32,33] It will be constructive if glioblastoma cells can be successfully detected on a trace scale. Thousands of lives will be saved by initiating the diagnosis of cancer.

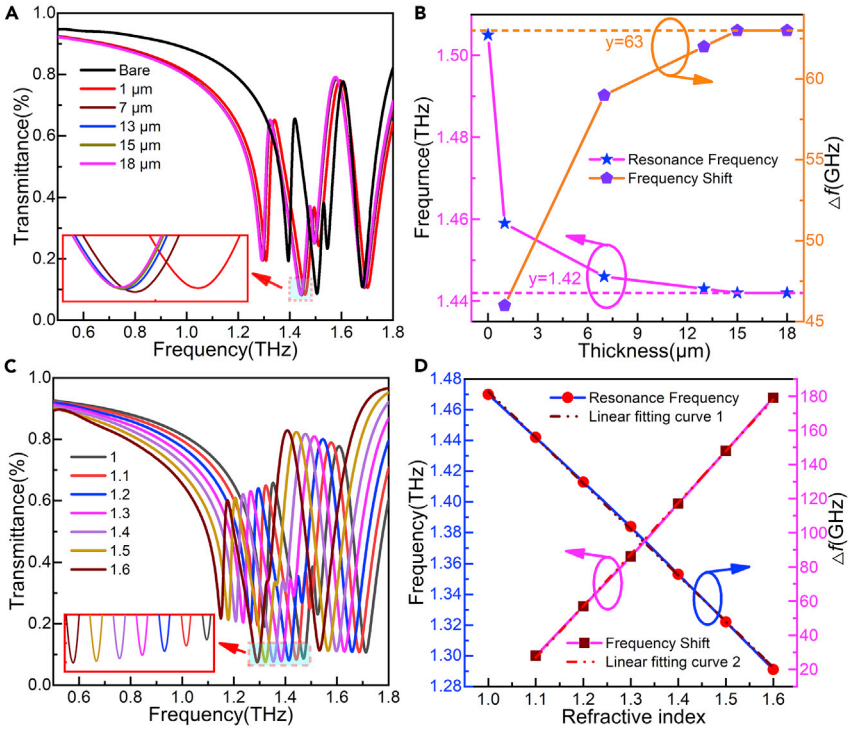

Figure 4. Theoretical sensitivity calculation

(A) The dependence of transmission on the analyte thickness increases from 1 μm to 18 μm under the fixed refractive index of 1.1.

(B) The resonance frequency and frequency shift under the different refractive indices of the analyte extracted from (A).

(C) The dependence of transmission of the analyte refractive index increases from 1 to 1.6 under the thickness of 15 μm.

(D) The resonance frequency and frequency shift under the different refractive indices of the analyte extracted from (C) and the corresponding linear fitting curves.

The method of glioblastoma cells cultured is as follow:

Glioblastoma cells in cryo-vial were thawed in a 37 °C water bath for no more than 1 min. Then these cells were transferred from the vial to a 15 mL sterile centrifuge tube, adding 3 mL pre-warmed cell culture medium, which consists of 90% DMEM (Dulbecco's modified eagle medium) high glucose liquid medium (Biosharp), 10% fetal bovine serum (Gibco) and Penicillin-Streptomycin (Macgene), after that the cells were centrifuged at 1000 rpm for 5 min. And then, we aspirate the supernatant, re-suspend the cells pellet in 4 mL cell culture medium and add re-suspended cells into a T25 flask. Finally, we placed the T25 flask in a 5% CO_2 incubator at 37 °C. The next day, the cell culture medium should be changed to ensure the normal and healthy growth of the cells. The cells need to be sub-cultured when the cell coverage in the dish reaches 80%-90%. Firstly, the cell culture medium should be removed, and the cell should be cleaned

Table 1. The comparison of the sensitivity of sensors based on metamaterials

Structure	Sensitivity(GHz/RIU)	Resonance type
[Structure 1][15]	76.5	Electric dipole Resonance
[Structure 2][29]	85	Electric Dipole Resonance
[Structure 3][31]	138	Electric Dipole Resonance
[Structure 4][30]	150	Fano resonance Resonance
[Structure 5][16]	182	Magnetic Dipole Resonance
[Structure 6][14]	248.8	EIT-like resonance Resonance
[Proposed Structure]	290	Electric Dipole Resonance

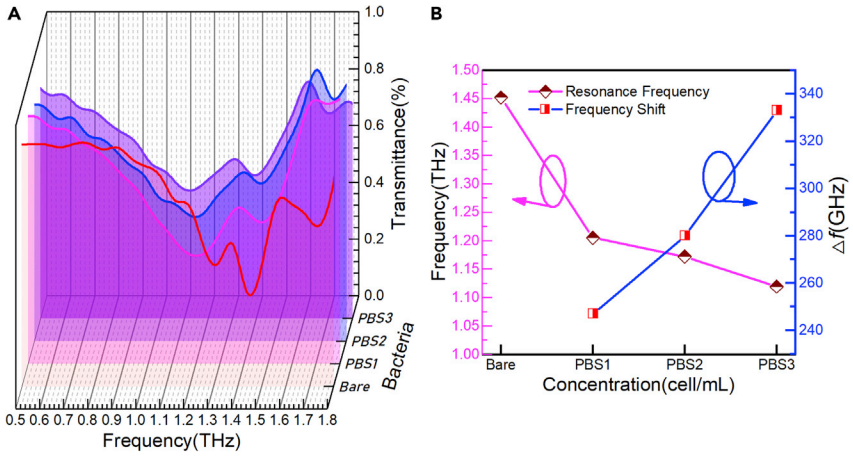

Figure 5. Concentration measurement

(A) The relationship between concentration and transmittance.

(B) The resonance peak frequency and Δf were extracted from (A).

with PBS. Then, incubate cells with 2 mL 0.25% Trypsin-EDTA solution (Gibco) for 2 min. As soon as cells have been detached, the cell culture medium should be added to end the digestive. Finally, Plating cells were in fresh flasks in a 5% CO_2 incubator at 37 °C. We harvest the cells and then digest the glioblastoma cells with 0.25% trypsin-EDTA (Gibco) and use the digested cells to prepare the 200 cells/mL concentration glioblastoma cells solution (Here, we take 1 μL glioblastoma solution under 1×10^5 cells/mL concentration condition drop into 1 mL deionized water to eliminate as much of the influence of culture fluid as possible. Also, the tested culture fluid is prepared in this way). The glioblastoma cell MMs biosensors have been prepared as mentioned previously. The measurement results are shown in Figure 7.

Unlike the measurement results in Figures 5 and 6, the resonance peak frequency no longer shifts hundreds of GHz compared with the bare one, as shown in Figure 7A. Also, with the peak frequency red shift, the amplitude is lower. However, the curves' amplitude will not be used as the feature to distinguish the analyte. Therefore, the frequency is limited from 1.36 THz to 1.49 THz to show the details, as shown in Figure 7B. The peak frequency decreases from about 1.45 THz to 1.44 THz when culture fluid is put on the MMs biosensor, the $\Delta f_c \approx 10$ GHz. Glioblastoma's resonance peak frequency lies at around 1.42 THz, $\Delta f_g \approx 30$ GHz.

The measurement results show that the two $\Delta f > 10$ GHz indicates that the MMs biosensor can detect culture fluid and glioblastoma. What is more, the frequency shifts between glioblastoma and culture fluid $|\Delta f_g - \Delta f_c| \geq 20$ GHz. The MMs biosensor does an excellent job; it can detect glioblastoma and culture fluid and distinguish glioblastoma and culture fluid under a low concentration condition. The MMs biosensor provides a simple and fast way for glioblastoma cell detection.

Conclusion

In this study, a kind of MMs based on the SRCCS structure has been proposed, and the MMs work in the THz regime. The structure consists of four split rings and a cross, and there are many gaps in this structure which means the capacitance C can be easily altered by filling these gaps with analytes. This property benefits to sensor because the resonance frequency is mainly determined by L and C, while the analyte can lead to a significant change in C. The influence of analyte layer thickness has been simulated, and the simulation results demonstrate that frequency shift Δf cannot be ignored until the analyte thickness reaches 15 μm. By fixing the thickness to 15 μm, the analyte refractive index changes from 1 to 1.6 to investigate the sensitivity of

Table 2. The Δf of its corresponding concentration and the calculated SoC

Δf (GHz)	250	280	330
Concentration (cells/mL)	PBS1 (2×10^5)	PBS2 (8×10^5)	PBS3 (1.2×10^6)
SoC (KHz·mL/cell)	1250	337.5	275

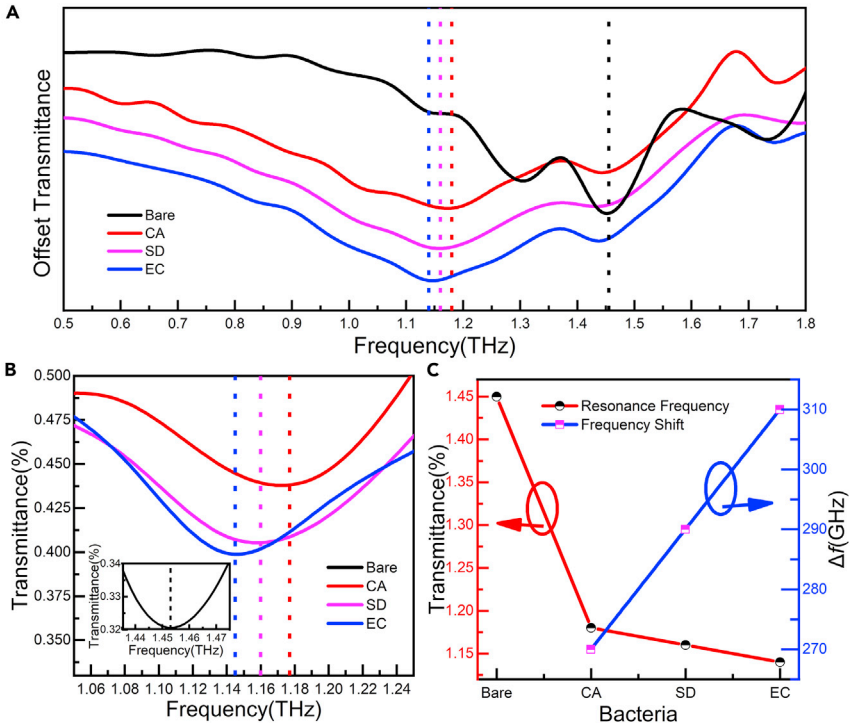

Figure 6. Different types of bacteria measurements

(A and B) The offset transmittance curves (A) and transmittance curves focus on frequency range from about 1.06 THz to 1.24 THz (B) of bare MMs biosensor and CA, SD, EC put onto MMs biosensor.

(C) The resonance peak frequency and Δf were extracted from (B).

the MMs sensor. The theoretical sensitivity of the MMs sensor is about 290 GHz/RIU. These hypothetical calculation results indicate that MMs can be used as a biosensor. In our experiment, with CA solution concentration improved from 2×10^5 cells/mL to 1.2×10^6 cells/mL, Δf changed from 250 GHz to 330 GHz. The experimental sensitivity of the MMs biosensor is not less than 275 kHz×mL/cell. Candida Albicans (CA), Escherichia Coli (EC), and *S. dysenteriae* (SD) are selected as analytes to verify the MMs biosensor's ability to detect and distinguish different types of bacteria which were selected due to the three kinds of differently sized bacteria. The experiment results show Δf_{CA} = 270 GHz, Δf_{SD} = 290 GHz, and Δf_{EC} = 310 GHz, which indicates that the MMs biosensor can detect and distinguish CA, EC, and SD Finally, glioblastoma cells solution with low-concentration culture fluid has been tested to check the possibility of working equally well with a low concentration of cells. The measurement results demonstrate that $\Delta f_c \approx 10$ GHz and $\Delta f_g \approx 30$ GHz, which reveals that the MMs

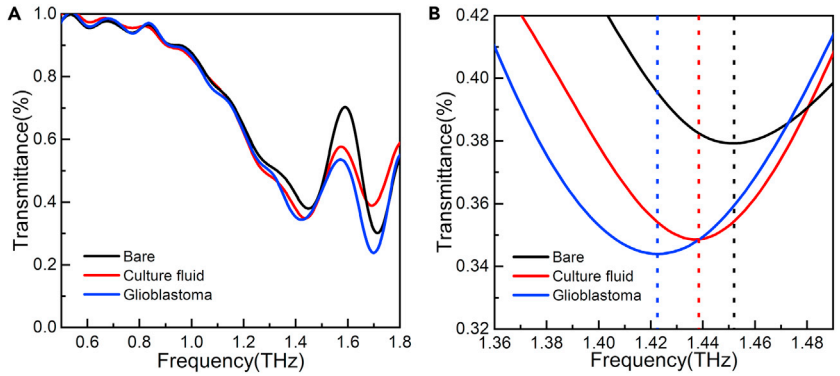

Figure 7. Cancer cells measurement

The transmittance curves of glioblastoma cells put on MMs biosensors (A) and transmittance curves focus on the range from 1.36 THz to 1.49 THz.

biosensor can detect low-concentration glioblastoma cells solution and culture fluid and distinguish them equally well. Neglect biological perspective, only counting the electromagnetic property of the analyte, the experiment certifies the MMs biosensor supplying a simple and fast way to bacteria and glioblastoma cell detection, which can be a huge milestone in the world of pathology.

Limitations of the study

In our study, we detected dry analytes to eliminate the effect of water. In that case, the bacteria cells and glioblastoma cells lose their biological activity, this study only counts the electromagnetic property of the analyte. Though the measurement results clarify the biosensor is very sensitive, the biological perspective of cells has been neglected. We will further study the biosensor which can sensitively detect and distinguish living cells.

STAR★METHODS

Detailed methods are provided in the online version of this paper and include the following:

- KEY RESOURCES TABLE
- RESOURCE AVAILABILITY
  - Lead contact
  - Materials availability
  - Data and code availability
- EXPERIMENTAL MODEL AND SUBJECT DETAILS
  - Bacteria preparation
  - Measurement setup
- METHOD DETAILS
  - Sensor preparation
  - Measurement steps
- QUANTIFICATION AND STATISTICAL ANALYSIS

ACKNOWLEDGMENTS

The authors thank Professor Xianlong Wei in Key Laboratory for the Physics and Chemistry of Nanodevices, School of Electronics Peking University, for fruitful discussions and encouragement. And thank Professor Xiaojun Wu, School of Electronic and Information Engineering, Beihang University for the experimental platform— the THz time-domain spectroscopy (THz-TDS). And thank Prof. J. Feng from the Vacuum Electronics National Laboratory, Beijing Vacuum Electronics Research Institute, China, for his sincere support for the research works in this article. We thank Prof. Xing-Ding Zhang (Sun Yat-sen University) for kindly providing GBM011 cells. The financial support provided by the National Natural Science Foundation of China (No. 61831001, 62005014), and supported by Beijing Natural Science Foundation Z200024 and Chinese Institute for Brain Research 2020-NKX-XM-04 is gratefully acknowledged.

AUTHOR CONTRIBUTIONS

Kanglong Chen (K.L.C.): conceptualization, design, experiment, writing – original draft. Cunjun Ruan (C.J.R.): supervision, investigation, writing – review & editing. Fanyuan Zhan (F.Y.Z.): fabrication, writing – review & editing. Xiaoyu Song (X.Y.S.): experiment, writing – review & editing. Ayesha Kosar Fahad (A.K.F.): writing – review & editing. Tianyao Zhang (T.Y.Z.): writing – review & editing. Wei Shi (W.S.): supervision, investigation, writing – review & editing.

DECLARATION OF INTERESTS

The authors declare no conflict of interest.

INCLUSION AND DIVERSITY

We support inclusive, diverse, and equitable conduct of research.

Received: September 5, 2022
Revised: November 30, 2022
Accepted: December 7, 2022
Published: January 20, 2023

REFERENCES

1. Ahmadivand, A., Gerislioglu, B., Ahuja, R., and Kumar Mishra, Y. (2020). Terahertz plasmonics: the rise of toroidal metadevices towards immunobiosensings. Mater. Today *32*, 108–130. https://doi.org/10.1016/j.mattod.2019.08.002.

2. Smith, D.R., Pendry, J.B., and Wiltshire, M.C.K. (2004). Metamaterials and negative refractive index. Science *305*, 788–792. https://doi.org/10.1126/science.1096796.

3. Ramakrishna, S.A. (2005). Physics of negative refractive index materials. Rep. Prog. Phys. *68*, 449–521. https://doi.org/10.1088/0034-4885/68/2/R06.

4. Makov, G., and Payne, M.C. (1995). Periodic boundary conditions in ab initio calculations. Phys. Rev. B Condens. Matter *51*, 4014–4022. https://doi.org/10.1103/PhysRevB.51.4014.

5. Leeuw, S.W.D., Perram, J.W., and Smith, E.R. (1980). Simulation of electrostatic systems in periodic boundary conditions. I. Lattice sums and dielectric constants. Proc. R. Soc. Lond. Math. Phys. Sci. *373*, 27–56. https://doi.org/10.1098/rspa.1980.0135.

6. Leeuw, S.W.D., Perram, J.W., and Smith, E.R. (1980). Simulation of electrostatic systems in periodic boundary conditions. II. Equivalence of boundary conditions. Proc. R. Soc. Lond. Math. Phys. Sci. *373*, 57–66. https://doi.org/10.1098/rspa.1980.0136.

7. De Leeuw, S.W., Perram, J.W., and Smith, E.R. (1983). Simulation of electrostatic systems in periodic boundary conditions. III. Further theory and applications. Proc. R. Soc. Math. Phys. Eng. Sci. *388*, 177–193.

8. Lee, Y., Kim, S.J., Park, H., and Lee, B. (2017). Metamaterials and metasurfaces for sensor applications. Sensors *17*, 1726. https://doi.org/10.3390/s17081726.

9. Chen, T., Li, S., and Sun, H. (2012). Metamaterials application in sensing. Sensors *12*, 2742–2765. https://doi.org/10.3390/s120302742.

10. Jakšić, Z., Vuković, S., Matovic, J., and Tanasković, D. (2010). Negative refractive index metasurfaces for enhanced biosensing. Materials *4*, 1–36. https://doi.org/10.3390/ma4010001.

11. Cao, J., Quan, B., Chen, K., Wang, B., Wang, L., and Wu, X. (2018). Towards ultra-strong terahertz field enhancement in nanogap split ring resonators. Opt. Info Base Conf. Pap. 9–11. https://doi.org/10.1364/isuptw.2018.wi12.

12. Yan, X., Yang, M., Zhang, Z., Liang, L., Wei, D., Wang, M., Zhang, M., Wang, T., Liu, L., Xie, J., and Yao, J. (2019). The terahertz electromagnetically induced transparency-like metamaterials for sensitive biosensors in the detection of cancer cells. Biosens. Bioelectron. *126*, 485–492. https://doi.org/10.1016/j.bios.2018.11.014.

13. Zhang, J., Mu, N., Liu, L., Xie, J., Feng, H., Yao, J., Chen, T., and Zhu, W. (2021). Highly sensitive detection of malignant glioma cells using metamaterial-inspired THz biosensor based on electromagnetically induced transparency. Biosens. Bioelectron. *185*, 113241. https://doi.org/10.1016/j.bios.2021.113241.

14. Yang, M., Liang, L., Zhang, Z., Xin, Y., Wei, D., Song, X., Zhang, H., Lu, Y., Wang, M., Zhang, M., et al. (2019). Electromagnetically induced transparency-like metamaterials for detection of lung cancer cells. Opt Express *27*, 19520–19529. https://doi.org/10.1364/oe.27.019520.

15. Lin, S., Xu, X., Hu, F., Chen, Z., Wang, Y., Zhang, L., Peng, Z., Li, D., Zeng, L., Chen, Y., and Wang, Z. (2021). Using antibody modified terahertz metamaterial biosensor to detect concentration of carcinoembryonic antigen. IEEE J. Select. Topics Quantum Electron. *27*, 1–7. https://doi.org/10.1109/JSTQE.2020.3038308.

16. Zhang, Z., Ding, H., Yan, X., Liang, L., Wei, D., Wang, M., Yang, Q., and Yao, J. (2018). Sensitive detection of cancer cell apoptosis based on the non-bianisotropic metamaterials biosensors in terahertz frequency. Opt. Mater. Express *8*, 659. https://doi.org/10.1364/ome.8.000659.

17. Haynes, W.M. CRC Handbook of Chemistry and Physics. 63.

18. Goodman, P. (2002). Current and future uses of gold in electronics. Gold Bull. *35*, 21–26. https://doi.org/10.1007/BF03214833.

19. Cao, W., Singh, R., Al-Naib, I.A.I., He, M., Taylor, A.J., and Zhang, W. (2012). Low-loss ultra-high-Q dark mode plasmonic Fano metamaterials. Opt. Lett. *37*, 3366–3368. https://doi.org/10.1364/ol.37.003366.

20. Cho, D.J., Wang, F., Zhang, X., and Shen, Y.R. (2008). Contribution of the electric quadrupole resonance in optical metamaterials. Phys. Rev. B *78*, 121101. https://doi.org/10.1103/PhysRevB.78.121101.

21. Pors, A., Nielsen, M.G., Della Valle, G., Willatzen, M., Albrektsen, O., and Bozhevolnyi, S.I. (2011). Plasmonic metamaterial wave retarders in reflection by orthogonally oriented detuned electrical dipoles. Opt. Lett. *36*, 1626–1628. https://doi.org/10.1364/ol.36.001626.

22. Hu, F., Xu, N., Wang, W., Wang, Y., Zhang, W., Han, J., and Zhang, W. (2016). A dynamically tunable terahertz metamaterial absorber based on an electrostatic MEMS actuator and electrical dipole resonator array. J. Micromech. Microeng. *26*, 025006. https://doi.org/10.1088/0960-1317/26/2/025006.

23. Liu, Y., and Zhang, X. (2011). Metamaterials: a new frontier of science and technology. Chem. Soc. Rev. *40*, 2494–2507. https://doi.org/10.1039/c0cs00184h.

24. Sabah, C., Mulla, B., Altan, H., and Ozyuzer, L. (2018). Cross-like terahertz metamaterial absorber for sensing applications. Pramana J. Phys. *91*, 17. https://doi.org/10.1007/s12043-018-1591-4.

25. Chen, H.-T., O'Hara, J.F., Taylor, A.J., Averitt, R.D., Highstrete, C., Lee, M., and Padilla, W.J. (2007). Complementary planar terahertz metamaterials. Opt Express *15*, 1084–1095. https://doi.org/10.1364/oe.15.001084.

26. Padilla, W.J., Aronsson, M.T., Highstrete, C., Lee, M., Taylor, A.J., and Averitt, R.D. (2007). Electrically resonant terahertz metamaterials: theoretical and experimental investigations. Phys. Rev. B *75*, 041102. https://doi.org/10.1103/PhysRevB.75.041102.

27. Zhang, C., Liang, L., Ding, L., Jin, B., Hou, Y., Li, C., Jiang, L., Liu, W., Hu, W., Lu, Y., et al. (2016). Label-free measurements on cell apoptosis using a terahertz metamaterial-based biosensor. Appl. Phys. Lett. *108*, 241105. https://doi.org/10.1063/1.4954015.

28. Smith, D.R., Gollub, J., Mock, J.J., Padilla, W.J., and Schurig, D. (2006). Calculation and measurement of bianisotropy in a split ring resonator metamaterial. J. Appl. Phys. *100*, 024507. https://doi.org/10.1063/1.2218033.

29. Li, Y., Chen, X., Hu, F., Li, D., Teng, H., Rong, Q., Zhang, W., Han, J., and Liang, H. (2019). Four resonators based high sensitive terahertz metamaterial biosensor used for measuring concentration of protein. J. Phys. D Appl. Phys. *52*, 095105. https://doi.org/10.1088/1361-6463/aaf7e9.

30. Geng, Z., Zhang, X., Fan, Z., Lv, X., and Chen, H. (2017). A route to terahertz metamaterial biosensor integrated with microfluidics for liver cancer biomarker testing in early stage. Sci. Rep. *7*, 16378. https://doi.org/10.1038/s41598-017-16762-y.

31. Sarkar, R., Devi, K.M., Ghindani, D., Prabhu, S.S., Chowdhury, D.R., and Kumar, G. (2020). Polarization independent double-band electromagnetically induced transparency effect in terahertz metamaterials. J. Opt. *22*, 035105. https://doi.org/10.1088/2040-8986/ab70f2.

32. Schwartzbaum, J.A., Fisher, J.L., Aldape, K.D., and Wrensch, M. (2006). Epidemiology and molecular pathology of glioma. Nat. Clin. Pract. Neurol. *2*, 494–503. https://doi.org/10.1038/ncpneuro0289.

33. Chen, R., Smith-Cohn, M., Cohen, A.L., and Colman, H. (2017). Glioma subclassifications and their clinical significance. Neurotherapeutics *14*, 284–297. https://doi.org/10.1007/s13311-017-0519-x.

34. Sevilla, M.J., and Odds, F.C. (1986). Development of Candida albicans hyphae in different growth media: variations in growth rates, cell dimensions and timing of morphogenetic events. J. Gen. Microbiol. *132*, 3083–3088. https://doi.org/10.1099/00221287-132-11-3083.

35. Germani, Y., and Sansonetti, P.J. (2006). The genus Shigella. In The Prokaryotes: A Handbook on the Biology of Bacteria Volume

6: Proteobacteria: Gamma Subclass, M. Dworkin, S. Falkow, E. Rosenberg, K.-H. Schleifer, and E. Stackebrandt, eds. (Springer New York), pp. 99–122. https://doi.org/10.1007/0-387-30746-X_6.

36. Balows, A., Trüper, H.G., Dworkin, M., Harder, W., and Schleifer, K.-H. (1992). The Prokaryotes: A Handbook on the Biology of Bacteria: Ecophysiology, Isolation, Identification, Applications (Springer).

37. Yang, P.D., Ouyang, C., Hong, T.S., Zhang, W.H., Miao, J.G., and Wu, X.J. (2020). Study of phase transition of single crystal and polycrystalline vanadium dioxide nanofilms by using continuous laser pump-terahertz probe technique. Acta Phys. Sin. *69*, 204205. https://doi.org/10.7498/aps.69.20201188.

38. Bai, Z., Liu, Y., Kong, R., Nie, T., Sun, Y., Li, H., Sun, T., Pandey, C., Wang, Y., Zhang, H., et al. (2020). Near-field terahertz sensing of HeLa cells and *Pseudomonas* based on monolithic integrated metamaterials with a spintronic terahertz emitter. ACS Appl. Mater. Interfaces *12*, 35895–35902. https://doi.org/10.1021/acsami.0c08543.

39. Fang, W., Lv, X., Ma, Z., Liu, J., Pei, W., and Geng, Z. (2022). A flexible terahertz metamaterial biosensor for cancer cell growth and migration detection. Micromachines *13*, 631. https://doi.org/10.3390/mi13040631.

STAR★METHODS

KEY RESOURCES TABLE

REAGENT or RESOURCE	SOURCE	IDENTIFIER
Bacterial and virus strains		
Candida Albicans	BEIJING MICROBIOLOGICAL CULTURE COLLECTION CENTER(BJMCC)	
Shigella Dysenteriae	BEIJING MICROBIOLOGICAL CULTURE COLLECTION CENTER(BJMCC)	
Escherichia Coli	BEIJING MICROBIOLOGICAL CULTURE COLLECTION CENTER(BJMCC)	
Biological samples		
Glioblastoma	Sun Yat-sen University Zhang Xingding lab	
Critical commercial reagent		
Bovine serum	Gibco	
Penicillin-Streptomycin	MACGENE Technology Ltd.	
Trypsin-EDTA	Gibco	
Deionized water	Aladdin	
DMEM	Life Technologies	
Deposited data		
iScience data	This paper	https://doi.org/10.17632/983fd2j3xc.1
Software and algorithms		
MATLAB R2020a	MathWorks Inc.	https://ww2.mathworks.cn/
CST STUDIO SUITE	3DEXPERIENCE Inc.	https://www.3ds.com/zh/products-services/simulia/products/cst-studio-suite/
Other		
Micro pipettes	Eppendorf	0.1–2.5 uL

RESOURCE AVAILABILITY

Lead contact

Further information and requests for resources and reagents should be directed to and will be fulfilled by the lead contact, Cunjun Ruan (ruancunjun@buaa.edu.cn).

Materials availability

This study did not generate new unique reagents.

Data and code availability

- This paper does not report original code.
- Any additional information required to reanalyze the data reported in this paper is available from the lead contact upon request.
- All simulation and measurement data have been uploaded to the Mendeley data (https://doi.org/10.17632/983fd2j3xc.1).

EXPERIMENTAL MODEL AND SUBJECT DETAILS

Earlier in the article, the measurement results confirmed that MM's fabrication meets the design and theoretical calculation, indicating that the MMs is promising for biosensor. Bacteria are chosen as analytes. The bacteria preparation, measurement methods, and experiment setup are as follows:

Bacteria preparation

The bacteria are bought from BEIJING MICROBIOLOGICAL CULTURE COLLECTION CENTER(BJMCC). The bacterial concentration of each type of original bacteriological sample is 1×10^8 cells/mL. Once the sample was thawed to room temperature, the OBS solution was dropped into 10 mL of deionized water using a liquid transfer gun to compound different concentration solutions (process bacteriological sample, PBS), as shown in table.

The OBS solution volume and PBS cells concentration

Serial Number	Cells concentration (cells/mL)
PBS1	2×10^5
PBS2	8×10^5
PBS3	1.2×10^6

Three types of bacteriological samples have been used as analytes in this experiment: Candida Albicans (CA), Shigella Dysenteriae (SD), and Escherichia Coli (EC). This selection was made due to their differences in sizes,[34–36] as shown in table.

The size of different types of bacteria

Bacteria types	CA	SD	EC
Size (nm)	3000–6000	1000 ~ 3000	50
D (nm)	6000		
G (nm)	5000		

Table tells us that size (S) relationship is $S_{CA} > S_{SD} > S_{EC}$. The various sizes will manifest that as electromagnetic properties vary, the number of bacteria cells filling the gap of MMs will differ to a large extent.

Measurement setup

THz time-domain spectroscopy (THz-TDS) has been employed to detect these sensors, as shown in figure.[37]

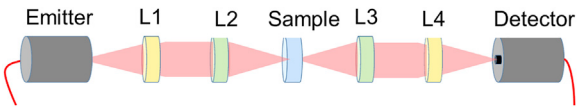

Experimental setup of optical modulation angle resolved terahertz time-domain spectroscopy

The fiber laser can generate 60 fs pulses with 1550 nm spectral width, and the power is 80 mW (FemtoFErb FD 6.5, Toptica Company). A horizontal polarization THz wave is generated when the laser drives on the InGaAs photoconductive antenna. The THz wave comes to parallel light when it passes through L1(collimating lens, the focal length f_1 = 50 mm), the parallel light passes through L2(condenser lens, the focal length f_2 = 100 mm) and then focused onto the sample. The THz wave passes through the sample and then goes through L3 (condenser lens, the focal length f_3 = 100 mm), and L4(collimating lens, the focal length f_4 = 50 mm). Finally, the receiver antenna will receive the THz wave signal, and the receiver antenna transforms THz radiation into a current signal. The THz radiation electric field vector can be detected by scanning Optical Delay Line and based on phase-locked amplifier technology. And the diameter of wave spot size is about 5 mm, which can ensure there are enough unit cells of metamaterial will in the THz wave radiation range.

METHOD DETAILS

Sensor preparation

Firstly, the fabricated MMs are sterilized with 75% ethanol and dried in a nitrogen environment at about 35 °C. Then, 1 mL PBS solution was shifted to the surface of the MMs biosensor to make sure the gold surface of the metamaterials was well-proportioned covered. The 1 mL solution will over-capacity to amplify the detection ability. Finally, the prepared sensors were placed at about 35 °C, and the nitrogen environment until these sensors were completely dry. At last, the bacteria film is finally formed. In some reports,

cells are cultured on the surface of metamaterial,[12–14,16,27,38,39] this method will cost a long time to culture cells, and the concentration is not accurate, also the water in cells will affect the measurement results. However, in our method, in the measurement the water effect can be eliminated, the detection time will shorten and the concentration is accurate. The HEK293T cell is selected as analyte to practice sensor preparation due to it is non-pathogenic properties. The micrograph of the MMs biosensor and with HEK293T (1×10^5 cells/mL) is shown in figure.

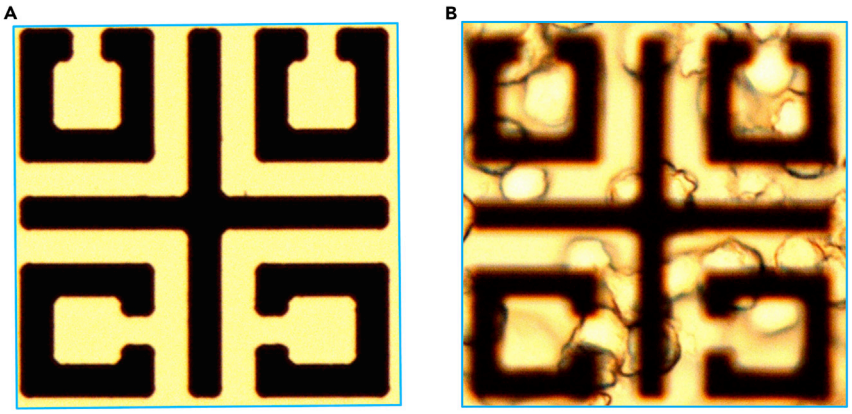

The SEM photograph of biosensor's unit cell
(A) The bare MMs biosensor.
(B) MMs biosensor with HEK293T cells.

Measurement steps

The completely dry biosensor is tested with the help of TDS, the spot of terahertz beam trapped in the metal shape part of the biosensor. To ensure the measurement results is accurate, we have selected the accurate timing window and scanning step width. Finally, we got the time domain spectral data. In the experiment, the scanning time is about 27 ps and 801 data points have been collected for each biosensor and bare substrate. The time domain spectral data was transformed to frequency domain spectral data (FDSD) by using the Fourier transform method. The transmittance spectral data is calculated by $Biosensor_{(FDSD)}/Substrate_{(FDSD)}$. Finally, the transmittance spectral data is processed by "B-spline" and transmittance curves of each biosensor have been plot.

QUANTIFICATION AND STATISTICAL ANALYSIS

The theoretical calculation was carried out by CST STUDIO SUITE, we use MW &RF &OPTICAL workflows, and Frequency Setup Solver. The boundary condition is unit cell in x and y directions, and open (add space) in z direction. The maximum step width is 0.1 μm, and the equation system solver accuracy is 1×10^{-9}. All these setting can make sure the simulation results are accurate. In our measurement, the resolution of our TDS is10 GHz, we Take the approximation of the resonance frequency, e.g., the bare biosensor resonance peak frequency is about 1.452 THz, we take it 1.45 THz. The error range of resonance frequency (n) is no more than 0.5%.